Energy transfer processes of Er^{3+} in $YAlO_3$

2003 J. Phys.: Condens. Matter 15 7423

(http://iopscience.iop.org/0953-8984/15/43/024)

INSTITUTE OF PHYSICS PUBLISHING JOURNAL OF PHYSICS: CONDENSED MATTER

J. Phys.: Condens. Matter **15** (2003) 7423–7436 PII: S0953-8984(03)67566-1

Energy transfer processes of Er^{3+} in $YAlO_3$

M Chua[1], S Xia[1,2] and P A Tanner[1]

[1] Department of Biology and Chemistry, City University of Hong Kong, Tat Chee Avenue, Hong Kong, SAR, People's Republic of China
[2] Structure Research Laboratory, Academica Sinica; Department of Physics, University of Science and Technology of China, Heifei, Anhui 230026, People's Republic of China

Received 12 August 2003
Published 17 October 2003
Online at stacks.iop.org/JPhysCM/15/7423

Abstract

In this study the upconversion of the $^4I_{13/2}$ and $^4I_{11/2}$ multiplets, and the cross-relaxation (CR) processes of $^4S_{3/2}$ and $^4I_{9/2}$ of Er^{3+} in $YAlO_3$, which are related to its 3 μm laser operation, have been investigated. The dominant energy transfer (ET) pathways are discussed and the ET rates of the contributing multipolar interaction mechanisms have been estimated, based upon the Holstein–Lyo–Orbach or the Miyakawa and Dexter formalisms for phonon-assisted ET. The Kushida formalism has been employed for the investigation of migration processes, and the matrix elements of Kaminskii for the relevant electronic transitions have been used in our calculations. The major results are that at room temperature, the contributions of $^2H_{11/2}$ (particularly from electric quadrupole–electric quadrupole interactions) to the CR and migration of $^4S_{3/2}$, and to the upconversion of $^4I_{11/2}$, are important, and are even the dominant ones in some cases.

1. Introduction

Since the theoretical treatment of sensitized luminescence by Förster [1] and Dexter [2], the study of energy transfer (ET) in rare earth phosphors has attracted much attention for its practical utility in laser materials. $YAlO_3$ is a well-known host lattice for rare earth ions, where the Y^{3+} cation can be replaced by, for example, Ce^{3+} [3], Pr^{3+} [4–7], Nd^{3+} [8], Eu^{3+} [9–12], Er^{3+} and Tm^{3+} [13]. In particular, Er^{3+} doped into $YAlO_3$ has aroused a great deal of research interest due to its 3 μm lasing, arising from the transitions between the $^4I_{11/2}$ and $^4I_{13/2}$ multiplets, as well as due to its green emission [14–19]. Silversmith *et al* [20] have developed the first continuous-wave $YAlO_3$:Er^{3+} upconversion laser. Five new 3 μm laser lines in $YAlO_3$:Er^{3+} are already being used in medical and biological applications [19]. This laser system is a peculiar one, since the lifetime of the upper laser level $^4I_{11/2}$ is smaller than that of the lower laser level $^4I_{13/2}$ [18]. Both the 3 μm laser and upconversion processes are only possible due to the high ET efficiency. For example, the upconversion rates of the $^4I_{13/2}$

and $^4I_{11/2}$ terms make important contributions to the dynamics of population inversion and the figure of merit of the 3 μm laser [19].

The number of possible ET pathways involved in any cross-relaxation (CR) or upconversion process between Er^{3+} ions may be rather greater than one. Estimating the dominant pathway is thus very complicated. Furthermore, the existence of multiple transfer processes such as looping mechanisms, photon avalanche, energy migration, and energy back transfer, etc, will further complicate the ET mechanisms. Microscopic semi-quantitative analysis is one of the possible means to determine the dominant ET pathway(s) that is/are really contributing to the respective process. Sufficient experimental results on the upconversion and CR rates of $YAlO_3$:Er^{3+} are now available, enabling us to perform a more detailed comparison with the theoretical analysis of the ET mechanisms and pathways in various processes [21–24].

In previous studies, the energy level structure relevant to the optical spectra of Er^{3+} in $YAlO_3$ has been thoroughly investigated [14–17, 19, 25]. Figure 1 labels the relevant SLJ multiplets discussed in this study and summarizes the spread of their energies. The scheme of the $^4I_{11/2} \rightarrow {}^4I_{13/2}$ $YAlO_3$:Er^{3+} 3 μm laser operation has been discussed elsewhere [26–28]. Recently, Kaminskii *et al* parametrized the intensities of bands in the absorption spectrum in the spectral region below 30 000 cm^{-1} [18], and presented all the reduced matrix elements between J-manifolds of the $4f^{11}$ configuration for Er^{3+} up to 97 000 cm^{-1}. These can be utilized in a theoretical estimation of ET rates.

In this paper, brief background discussions of the $YAlO_3$ crystal structure and phonon density of states, and of various theories of ET, are presented in sections 2 and 3, respectively. In section 4, the various ET processes involved in the dynamics of population inversion of the 3 μm laser of Er^{3+} in $YAlO_3$, CR from $^4S_{3/2}$, upconversion from $^4I_{13/2}$ and from $^4I_{11/2}$, which also contribute to its figure of merit, are calculated and discussed. In section 5, the CR from $^4I_{9/2}$ is studied, since this has detrimental effects upon the oscillation threshold of the laser, with increasing Er^{3+} concentration. The major results are summarized in section 6.

2. $YAlO_3$ crystal structure and phonon density

$YAlO_3$ crystallizes in a distorted perovskite structure, in the space group $Pnma$-D_{2h}^{16} (No 62), $Z = 4$, and the details of the crystal structure have been given in [29–33]. The unit cell comprises four perovskite-like pseudocells. A sketch is given in figure 2, showing the orthorhombic unit cell ($a = 0.5330$ nm, $b = 0.7375$ nm, $c = 0.5180$ nm) and a subunit corresponding to the ideal cubic perovskite unit cell. The structure of $Y_{0.5}Er_{0.5}AlO_3$ has also been reported [34].

In $YAlO_3$, the Y^{3+} ion occupies each of the eight corners of the pseudocell; O^{2-} each of the six face centres, and Al^{3+} the body centre. Certain dimensions are required in our subsequent calculations. The chain Al^{3+}–O^{2-}–Al^{3+} is parallel to the c crystal axis, and the distance within the Y^{3+}–Y^{3+} chain is 0.3758 nm [32]. The corresponding number of neighbours with this separation is 6. The a and b directions of the unit cell are parallel to [110] and [$\bar{1}$10] of the pseudocell, respectively. The mean Y^{3+}–O^{2-} distances of the bond chains Y^{3+}–O^{2-}–Y^{3+} parallel to the a and the b crystal axes are 0.2634 and 0.2689 nm respectively [32]. The average Y^{3+}–O^{2-}–Y^{3+} distance is $\sqrt{2} \times 0.3758 = 0.5314$ nm and the number of neighbours with this separation is 12. The third nearest neighbour distance of Y^{3+}, in the set of 8, is $\sqrt{3} \times 0.3758 = 0.6508$ nm along the bond chain Y^{3+}–Al^{3+}–Y^{3+}.

The phonon spectrum of $YAlO_3$ has cutoff frequency $\approx$800 cm^{-1} [35, 36], with Debye temperature $\theta_D \approx 1150$ K [37]. In comparison with the effective phonon density of cubic $Y_3Al_5O_{12}$, (YAG), where the cutoff frequency is $\approx$500 cm^{-1} and $\theta_D \approx 700$ K [38], the phonon density of states in $YAlO_3$ is more expansive and favourable for the operation of

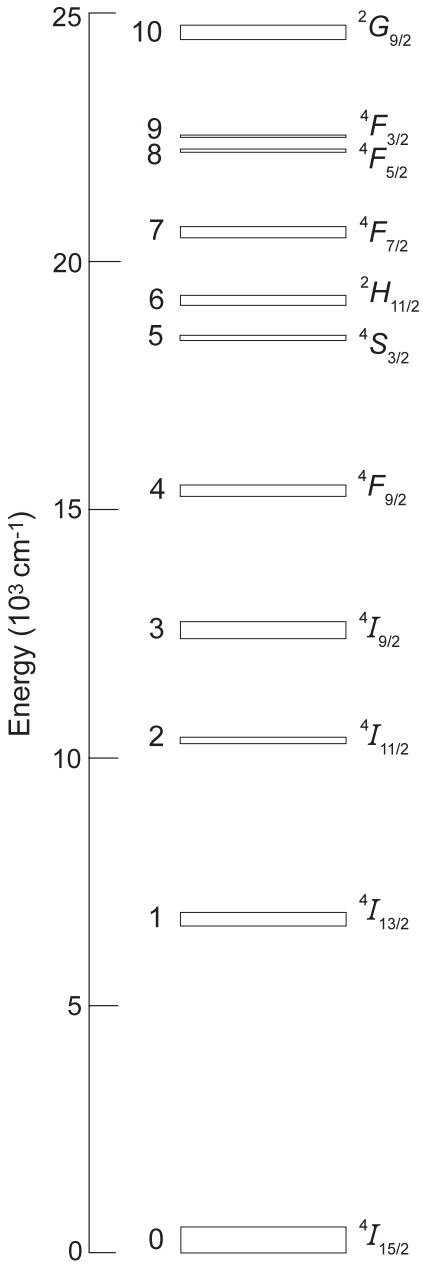

Figure 1. The energy level scheme of Er^{3+} in $YAlO_3$.

phonon-assisted ET processes. Nonradiative processes of various rare earth ions doped into $YAlO_3$ have been studied by Weber [17].

3. Theory of energy transfer (ET) processes

The theory of resonant ET processes was first formulated by Förster [1] and Dexter [2]. Kushida [39] then generalized the theory to calculate the averaged rate $\bar{P}_{AB}$ of ET between the

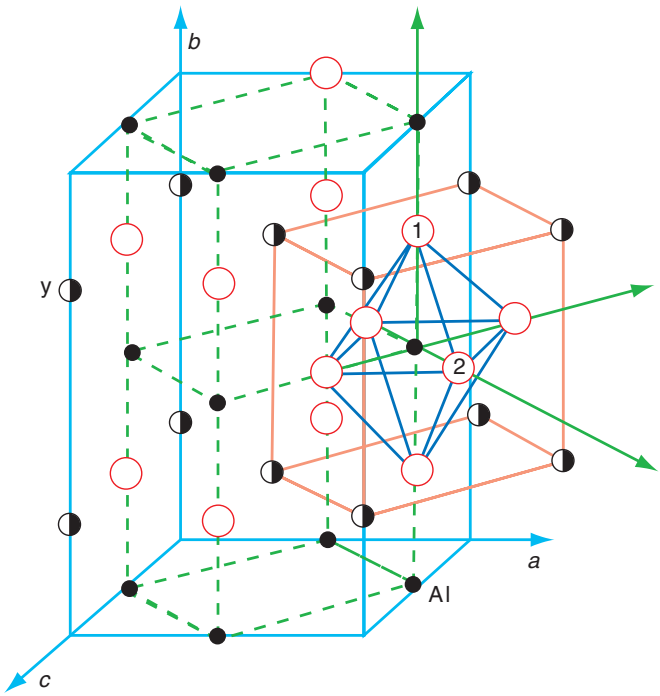

Figure 2. Crystal structure of $YAlO_3$. The two types of oxygen are labelled 1 and 2. (This figure is in colour only in the electronic version)

manifolds J_a and J_b by summing over all the possible terminal crystal field (CF) states $|a'b'\rangle$ and taking the Boltzmann-weighted average of the initially occupied CF states, $|ab\rangle$:

$$\bar{P}_{AB} = \frac{2\pi}{\hbar}\overline{J^2}\bar{S}, \tag{1}$$

where:

$$\overline{J^2} = \frac{1}{[J_a][J_b]} \sum_{\substack{a,b \\ a',b'}} |\langle ab|H_{AB}|a'b'\rangle|^2 \tag{2}$$

is the 'squared electronic transition element', averaged over the initial CF states but summed over the terminal CF states, for ET between the manifolds J'_a and J'_b.

$$\bar{S} = \frac{1}{[J'_a][J'_b]} \sum_{\substack{a,b \\ a',b'}} Y_a Y_b \int g_{aa'}(E) g_{bb'}(E)\, \mathrm{d}E \tag{3}$$

is the averaged overlap integral between individual CF emission and individual CF absorption transitions, in which $[J] = 2J + 1$, Y is a normalized Boltzmann factor, and g is a line shape function. The typical value of $\bar{S}$ at room temperature is $1 \times 10^{-3}/\mathrm{cm}^{-1}$ [39], which will be used in this paper for ET migration between manifolds.

Depending upon the different interaction mechanisms, the $\overline{J^2}$ can be calculated by different formulae as follows:

$$\overline{J^2} = \frac{1}{[J_a][J_b]}\left(\frac{14}{5}\right)\left(\frac{e^4}{R^{10}}\right) \times \langle 4f|r_A^2|4f\rangle^2 \langle 4f|r_B^2|4f\rangle^2 \langle f||C^{(2)}||f\rangle^4 \langle J_a||U^{(2)}||J'_a\rangle^2 \langle J_b||U^{(2)}||J'_b\rangle^2, \tag{4}$$

for electric quadrupole–electric quadrupole (qq) interaction between the donor and acceptor, with separation R, where $\langle J||U^{(2)}||J'\rangle$ is the reduced matrix element of the unit tensor $U^{(2)}$;

$$\overline{J^2} = \frac{1}{[J_a][J_b]}\left(\frac{2}{3}\right)\left(\frac{e^4}{R^6}\right)\left[\sum_\lambda \Omega_{A\lambda}\langle J_a||U^{(\lambda)}||J'_a\rangle^2\right]\left[\sum_\lambda \Omega_{B\lambda}\langle J_b||U^{(\lambda)}||J'_b\rangle^2\right], \tag{5}$$

for electric dipole–electric dipole (dd) interaction, where Ω_λ ($\lambda = 2, 4, 6$) is the Judd parameter obtained by fitting manifold–manifold ED transition intensities;

$$\overline{J^2} = \frac{1}{[J_a][J_b]}\left(\frac{e^4}{R^8}\right)\left[\sum_\lambda \Omega_{A\lambda}\langle J_a||U^{(\lambda)}||J'_a\rangle^2\right]\langle 4f|r_B^2|4f\rangle^2\langle f||C^{(2)}||f\rangle^2\langle J_b||U^{(2)}||J'_b\rangle^2, \tag{6}$$

for dq interaction;

$$\overline{J^2} = \frac{1}{[J_a][J_b]}\left(\frac{e^4}{R^8}\right)\langle 4f|r_A^2|4f\rangle^2\langle f||C^{(2)}||f\rangle^2\langle J_a||U^{(2)}||J'_a\rangle^2\left[\sum_\lambda \Omega_{B\lambda}\langle J_b||U^{(\lambda)}||J'_b\rangle^2\right], \tag{7}$$

for qd interaction.

These equations will be used in the present work, in which the values of the intensity parameters Ω_λ and the squared reduced elements of $U^{(\lambda)}$ are taken from the work of the Kaminskii group [18].

The analysis of nonresonant ET processes has been performed by Holstein *et al* [40] and Miyakawa and Dexter [41], and the proposed mechanisms are subsequently denoted as HLO and MD respectively. In the HLO mechanism the diagonal one-phonon-assisted transition rate of ET between CF energy states for a large energy mismatch is given by [40]:

$$W = \frac{J^2(f_e - f_g)^2|\Delta E|}{\pi\hbar^4\rho}\left(\sum_s \frac{\alpha_s}{v_s^5}\right)\left\{\begin{matrix} n+1 \\ n \end{matrix}\right\}, \tag{8}$$

where J^2 is the squared matrix element of the electronic transition between the CF states $|ab\rangle$ and $|a'b'\rangle$ and $(f_e - f_g)$ is the difference between the ion–phonon coupling strength of the excited and ground states, assumed approximately to be the same for the donor and acceptor. In this work we take the value 200 cm^{-1} for $(f_e - f_g)$, since $f \sim 1000$ cm^{-1} for rare earth optical transitions [40], ΔE is the energy mismatch between sites, ρ is the mass density, v_s is the phonon velocity, and α_s, the angular average of the strain tensor, is of order unity. The terms $n+1$ and n in the curly bracket refer to phonon emission and absorption, respectively, where n is the average number of phonons at temperature T. For the studied rate of manifold–manifold ET, the summation over terminal CF states needs to be employed, with the average over the initial CF states, i.e.:

$$\bar{P}_{AB} = W\left(\frac{\overline{J^2}}{J^2}\right). \tag{9}$$

The alternative MD model [41] of nonresonant ET, based on the 'energy gap dependence', provides an expression for the rate of ET between CF states, similar to that for phonon relaxation processes, given as:

$$W = W(0)\exp(-\beta\Delta E) \tag{10}$$

where

$$W(0) = \frac{2\pi}{\hbar}|H_{ab}|^2\sigma_{ab}\exp[-(g_a + g_b)], \tag{11}$$

$|H_{ab}|^2 = J^2$, which should be changed to $\overline{J^2}$ as in equation (9) for manifold–manifold ET, σ_{ab} is the overlap integral between the zero phonon line peaks of the CF emission and CF absorption spectra when the energy mismatch is zero, and we take its estimated value to be $4 \times 10^{-3}/\mathrm{cm}^{-1}$ at room temperature, and the so-called electron–lattice coupling constant $g = S_0(2n + 1)$, in which S_0 is the Huang–Rhys factor for the effective phonon. If we take $S_0 = 0.05$, $\hbar\omega_{\mathrm{eff}} = 600\ \mathrm{cm}^{-1}$ [17], then $g = 0.057$ at room temperature.

The parameter β in equation (10) is related to the parameter α used in the 'energy gap dependence' of the multiphonon relaxation rate as follows:

$$\beta = \alpha - \gamma, \tag{12}$$

where

$$\alpha = \frac{1}{\hbar\omega}\left[\ln\frac{N}{g(n+1)} - 1\right], \tag{13}$$

and

$$\gamma = \frac{1}{\hbar\omega}\ln\left(1 + \frac{g_b}{g_a}\right), \tag{14}$$

where N is the number of phonons emitted in the process.

For $YAlO_3$, Weber gave $\hbar\omega_{\mathrm{eff}} = 600\ \mathrm{cm}^{-1}$, $\alpha = 0.046$ cm, at 77 K [17]. If we take $N = 3$, then $g = 0.07$ from equation (13); as an estimated value, we take the average of 0.057 and 0.07, i.e. we employ $g_a = g_b = 0.064$ in the following discussion. Yamada *et al* [42] have shown that the MD energy gap law is applicable to rare earth ions diluted into Y_2O_3, since experimental data indicate that the ET rate is mainly governed by the magnitude of the energy gap.

In the following calculation, we consider a donor ion which transfers its energy to the acceptor ions located as first, second and third neighbours, and hence the ET rate is expressed as:

$$\bar{P}_{\mathrm{total}} = \sum_{S=1}^{3} \bar{P}_{AB}(R_S) N_S C_{\mathrm{Er}} P_a, \tag{15}$$

where $\bar{P}_{AB}(R_S)$ is the ET rate for the donor–acceptor pair at a separation of R_S, and the shell index, S, runs from the first to the third nearest neighbours, N_S is the number of the acceptor ions in the S shell; C_{Er} is the concentration of Er^{3+} doping, and P_a is the probability that the acceptor ion is in the initial state of the relevant ET process.

Based upon the crystal structure mentioned above, we have $N_1 = 6$, $N_2 = 12$, $N_3 = 8$, and $R_2 = \sqrt{2}R_1$, $R_3 = \sqrt{3}R_1$. Since $\bar{P}_{AB}(R_S)$ is proportional to $\overline{J^2}$, which depends upon the donor–acceptor distance R as shown in equations (4)–(7), the summation in (15) is:

$$\sum_{S=1}^{3} \bar{P}_{AB}(R_S) N_S = \left[6 + 12\left(\frac{1}{\sqrt{2}}\right)^6 + 8\left(\frac{1}{\sqrt{3}}\right)^6\right] \bar{P}_{AB}(R_1) = 8\bar{P}_{AB}(R_1) = 8\bar{P}_{\mathrm{dd}}(R_1) \tag{16}$$

for dd interaction ET,

$$\begin{aligned}\sum_{S=1}^{3} \bar{P}_{AB}(R_S) N_S &= \left[6 + 12\left(\frac{1}{\sqrt{2}}\right)^8 + 8\left(\frac{1}{\sqrt{3}}\right)^8\right] \bar{P}_{AB}(R_1) = 6.85\bar{P}_{AB}(R_1) \\ &= 6.85\bar{P}_{\mathrm{dq}}(R_1) \qquad \text{or} \qquad 6.85\bar{P}_{\mathrm{qd}}(R_1)\end{aligned} \tag{17}$$

for dq or qd interaction ET,

$$\sum_{S=1}^{3} \bar{P}_{AB}(R_S)N_S = \left[6 + 12\left(\frac{1}{\sqrt{2}}\right)^{10} + 8\left(\frac{1}{\sqrt{3}}\right)^{10}\right]\bar{P}_{AB}(R_1)$$
$$= 6.41\bar{P}_{AB}(R_1) = 6.41\bar{P}_{\mathrm{qq}}(R_1) \tag{18}$$

for qq interaction ET transfer. Therefore we have

$$\bar{P}_{\mathrm{total}} = \{8\bar{P}_{\mathrm{dd}}(R_1) + 6.85[\bar{P}_{\mathrm{dq}}(R_1) + \bar{P}_{\mathrm{qd}}(R_1)] + 6.41\bar{P}_{\mathrm{qq}}(R_1)\}C_{\mathrm{Er}}P_a. \tag{19}$$

4. Concentration quenching and upconversion processes of Er^{3+} in $YAlO_3$

In this section, we will investigate the upconversion processes of $^4I_{13/2}$ and $^4I_{11/2}$, and CR processes of $^4S_{3/2}$. The purpose of the semi-quantitative calculations is to identify the dominant interaction mechanism(s) and pathway(s) in each of the examined ET processes. Effective field corrections and screening effects in the ET to more distant acceptors have not been considered. The relatively less important contributions from nondiagonal phonon-assisted processes have not been especially considered, but for dipole transitions, they have been contained in the fitting values of the parameters Ω_λ. At the C_s symmetry site where Er^{3+} substitutes for Y^{3+}, electric dipole transitions between levels of the $4f^{11}$ electronic configuration of Er^{3+} are enabled by the odd parity CF terms, which are the main contributors to the parameters Ω_λ.

4.1. The concentration quenching of the $^4S_{3/2}$ state

Under xenon flash lamp pumping, the $^4S_{3/2}$ level plays the role of the 3 μm laser pumping level. The lifetime of this state in a 0.5 at.% Er^{3+}-doped crystal is 120 μs at 300 K, and the estimated radiative quantum efficiency is 0.32 [37, 43]. The luminescence lifetime, τ, of this energy level depends strongly on the Er^{3+} doping concentration, C_{Er}. For YAG, τ decreases by more than two orders of magnitude when C_{Er} increases from 0.1 to 100 at.% [43]. For $YAlO_3$, the quenching is more pronounced, with τ decreasing by more than three orders with C_{Er} increasing from 0.1 to 45 at.%. This effect has been attributed to the following CR process [44, 45]:

$$\mathrm{CR}_{5\to3,0\to1}: [^4S_{3/2}, {}^4I_{15/2}] \to [^4I_{9/2}, {}^4I_{13/2}] \qquad (-1194, +8\ \mathrm{cm}^{-1}), \tag{20}$$

where the CR subscripts denote the decay of the donor ion from the energy level 5 to 3 (notation as in figure 1) and the transfer of energy which excites the acceptor ion from level 0 to 1. In this equation, and in the following, the energy mismatches indicated in the parenthesis represent the minimum and maximum values for individual CF transitions, with + and − denoting phonon emission and absorption, respectively. In the following calculations we have taken the baricentred average values of energy mismatch. Examination of the energy level scheme leads to the suggestion of other possible CR pathways:

$$\mathrm{CR}_{5\to1,0\to3}: [^4S_{3/2}, {}^4I_{15/2}] \to [^4I_{13/2}, {}^4I_{9/2}] \qquad (-1194, +8\ \mathrm{cm}^{-1}), \tag{21}$$

$$\mathrm{CR}_{5\to2,0\to1}: [^4S_{3/2}, {}^4I_{15/2}] \to [^4I_{11/2}, {}^4I_{13/2}] \qquad (+1136, +2119\ \mathrm{cm}^{-1}), \tag{22}$$

as well as double excitations (upconversions) from $^4S_{3/2}$, which we do not consider here. Contributions of the processes (20)–(22) to the quenching of $^4S_{3/2}$ emission are now considered individually below.

For the 1.5 at.% Er^{3+} system, at 300 K the measured lifetime of $^4S_{3/2}$ and the quenching efficiency were found to be 70 μs and 53%, respectively [45], with the quenching rate estimated

Table 1. Squared interaction matrix elements ($\times 10^{-50}$ J^2) for transfer to first nearest-neighbours (at 0.3758 nm) of selected ET processes of Er^{3+} in $YAlO_3$.

ET process	Equation	Squared interaction matrix element ($\times 10^{-50}$ J^2) $\overline{J^2}$ (dd)	$\overline{J^2}$ (dq)	$\overline{J^2}$ (qd)	$\overline{J^2}$ (qq)	Total ($\times 10^{-50}$ J^2)	Comments
$[^4S_{3/2}, {}^4I_{15/2}] \rightarrow [^4I_{9/2}, {}^4I_{13/2}]$	(20)	3.20	7.59	0	0	10.79	dq > dd
$[^4S_{3/2}, {}^4I_{15/2}] \rightarrow [^4I_{13/2}, {}^4I_{9/2}]$	(21)	0.398	0	0	0	0.398	dd
$[^4S_{3/2}, {}^4I_{15/2}] \rightarrow [^4I_{11/2}, {}^4I_{13/2}]$	(22)	0.751	1.76	0	0	2.51	dq > dd
$[^2H_{11/2}, {}^4I_{15/2}] \rightarrow [^4I_{9/2}, {}^4I_{13/2}]$	(23)	2.26	5.36	127	563	697	qq > qd > dq > dd
$[^2H_{11/2}, {}^4I_{15/2}] \rightarrow [^4I_{13/2}, {}^4I_{9/2}]$	(24)	0.0601	0	1.70	0	1.76	qd > dd
$[^2H_{11/2}, {}^4I_{15/2}] \rightarrow [^4I_{11/2}, {}^4I_{13/2}]$	—	6.61	481	481	70 600	71 200	qq > qd = dq > dd
$[^4I_{13/2}, {}^4I_{13/2}] \rightarrow [^4I_{15/2}, {}^4I_{9/2}]$	(25)	2.26	0.24	5.35	1.06	8.91	qd > dd > qq > dq
$[^4I_{9/2}, {}^4I_{15/2}] \rightarrow [^4I_{13/2}, {}^4I_{13/2}]$	(28)	2.77	6.55	0.294	1.30	10.9	dq > dd > qq > qd
$[^4I_{11/2}, {}^4I_{11/2}] \rightarrow [^4I_{15/2}, {}^4F_{7/2}]$	(26)	0.515	0.798	6.32	18.3	25.9	qq > qd > dq > dd
$[^4I_{11/2}, {}^4I_{11/2}] \rightarrow [^4I_{15/2}, {}^2H_{11/2}]$	(27)	0.287	8.01	3.49	183.5	195.3	qq > qd > dq > dd

$\sim 10^4$ s^{-1}. The processes $CR_{5\rightarrow 3,0\rightarrow 1}$ and $CR_{5\rightarrow 1,0\rightarrow 3}$ each require one phonon absorption (taken as $\sim$400 cm^{-1}) to bridge the energy mismatch. The short-lived state $^4I_{9/2}$ relaxes nonradiatively to $^4I_{11/2}$, so that the same terminal states, $^4I_{13/2}$ and $^4I_{11/2}$, are populated in processes (20) and (21), as in process (22). On the other hand, the process (22), $CR_{5\rightarrow 2,0\rightarrow 1}$, involves the emission of three phonons to assist the ET process. Two points should be noted here: (i) the individual contributions of these three processes have not been distinguished from experimental measurements, although (22) would completely bypass $^4I_{9/2}$ so that much weaker emission would be expected from $^4I_{9/2}$, compared with processes (20) and (21). (ii) These three CR processes of $^4S_{3/2}$ will not enhance the 3 μm lasing efficiency because the terminal states $^4I_{11/2}$ and $^4I_{13/2}$ (i.e. the initial and terminal lasing levels) are approximately equally populated.

For the first CR process, $CR_{5\rightarrow 3,0\rightarrow 1}$, the quadrupole transition of the donor ion from $^4S_{3/2}$ to $^4I_{9/2}$ is forbidden, and hence only the dd and dq interactions are active. The squared electronic transition matrix elements $\overline{J^2}(R_1)$ calculated by (5) and (6) using the data of [18], and $\langle r^2 \rangle = 0.831\ a_0^2$, are given in table 1. Using the HLO formalism, equation (8), and employing $v_S = 2 \times 10^3$ s^{-1}, $\rho \approx 5 \times 10^3$ kg m^{-3}, and $(f_e - f_g) = 200$ cm^{-1}, the ET rate for 1.5% doping is found to be 3960 s^{-1}, and is one order smaller than the experimental result. The ET rates due to dd and dq interaction mechanisms are found to be comparable. For the process in (21), $CR_{5\rightarrow 1,0\rightarrow 3}$, only the dd interaction mechanism is active since both the quadrupole transitions from $^4S_{3/2}$ to $^4I_{13/2}$ and $^4I_{15/2}$ to $^4I_{9/2}$ are forbidden (the $\overline{J^2}$ are listed in table 1). The estimated CR rate of this process (21) is 160 s^{-1}, which is 25 times smaller than the process $CR_{5\rightarrow 3,0\rightarrow 1}$. Finally, for process (22), $CR_{5\rightarrow 2,0\rightarrow 1}$, both the qd and qq interactions are inactive because the $^4S_{3/2}$ to $^4I_{11/2}$ quadrupole transition is forbidden, and the calculated nonzero $\overline{J^2}$ are shown in table 1. Since this ET process involves the emission of 3 phonons, we will employ the MD model, equation (10), to estimate the ET rate. First of all, when we take the overlap integral to be 4×10^{-3}/cm^{-1}, the resonant ET rate $W(0)$ is found to be 2.8×10^4 s^{-1}. The α and β factors calculated by (13) and (12) for an energy mismatch of 1750 cm^{-1} (=3 $\hbar\omega$) and temperature 300 K, are estimated to be 4.8×10^{-3} and 3.6×10^{-3}, respectively. The exponential factor of (10) then equals 1.84×10^{-3} and the CR rate of process $CR_{5\rightarrow 2,0\rightarrow 1}$ is 52 s^{-1}. In all, the CR process (20) $CR_{5\rightarrow 3,0\rightarrow 1}$ really dominates over the other two processes (21), (22), but is still an order smaller than the experimental result.

Since the $^2H_{11/2}$ state, between 632 cm^{-1} (shortest gap between individual CF levels) to 897 cm^{-1} (largest gap) above the $^4S_{3/2}$ state, is thermally populated at 300 K, it is of interest to investigate the contribution of this multiplet to the quenching process of $^4S_{3/2}$ [23]. Assuming that the states are in thermal equilibrium and according to Boltzmann distribution, based upon the detailed energy data of the CF states of $^2H_{11/2}$ and $^4S_{3/2}$ [22], it is found that about 8% of the $^4S_{3/2}$–$^2H_{11/2}$ excited donor ion is populated in the $^2H_{11/2}$ state. The initial energy states involved in the two ET processes, $CR_{5\rightarrow3,0\rightarrow1}$ and $CR_{5\rightarrow1,0\rightarrow3}$, are then $^2H_{11/2}$ instead of $^4S_{3/2}$ and these processes are re-written as:

$$CR_{6\rightarrow3,0\rightarrow1}: [^2H_{11/2}, {}^4I_{15/2}] \rightarrow [^4I_{9/2}, {}^4I_{13/2}] \qquad (-481, +824\ cm^{-1}), \quad (23)$$

$$CR_{6\rightarrow1,0\rightarrow3}: [^2H_{11/2}, {}^4I_{15/2}] \rightarrow [^4I_{13/2}, {}^4I_{9/2}] \qquad (-481, +824\ cm^{-1}). \quad (24)$$

Each of these two processes requires one phonon emission to bridge the energy mismatch, taken as ∼400 cm^{-1}. For the third ET process (22), $CR_{5\rightarrow2,0\rightarrow1}$, if $^2H_{11/2}$ is involved rather than $^4S_{3/2}$ then the energy mismatch (between 1849 and 2935 cm^{-1}) requires the emission of four phonons.

For process (23), $CR_{6\rightarrow3,0\rightarrow1}$, all the dd, dq, qd and qq interactions are active. The squared reduced matrix element of the donor transition, $|\langle^2H_{11/2}||U^{(2)}||^4I_{9/2}\rangle|^2 = 0.2077$, is comparatively large and hence qq and qd interactions are expected to be the dominant interaction mechanisms in this case, as shown in table 1. Using the HLO formalism, the quenching rate for 1.5% Er^{3+} doping is calculated to be 1.3×10^5 s^{-1}. The quenching rate for process (24), $CR_{6\rightarrow1,0\rightarrow3}$ is 342 s^{-1}, which is more than two orders slower (table 1). Hence (23), $CR_{6\rightarrow3,0\rightarrow1}$ is the dominant pathway that accounts for the quenching process. The lifetime of $^4S_{3/2}$ in $YAlO_3$:Er^{3+} with 2% Er^{3+} doping, is shortened to 50 μs [46], and the calculated CR rate is 5.5×10^4 s^{-1}.

For the higher dopant ion concentration of 45% Er^{3+}, the measured lifetime of the $^4S_{3/2}$ state is as short as 0.1 μs [44]. This requires the quenching rate to be as large as 10^7 s^{-1}. The ET rate under this doping concentration due to process $CR_{6\rightarrow3,0\rightarrow1}$ is estimated to be 3.9×10^6 s^{-1} and the corresponding lifetime is calculated to be 0.26 μs. The agreement is reasonable within the model framework, but the difference could also be attributed to several factors, including the energy migration to killer or trap sites, so that we now estimate the energy migration rate to see if the latter quenching mechanism may be of importance.

The reduced matrix element of $|\langle^2H_{11/2}||U^{(2)}||^4I_{15/2}\rangle|^2 = 0.7125$ is extremely large, and therefore the qq migration matrix element is extremely large (table 1). Notably, the reduced matrix element is much larger than for other spin-forbidden transitions, such as for Tb^{3+} where the squared reduced $U^{(2)}$ matrix element of $^7F_6$ to $^5D_4$ is 7.3×10^{-4} [47], using the wavefunctions reported by Ofelt [48], and for Eu^{3+} it is 8×10^{-4} [49]. For 45% Er^{3+} dopant ion concentration, the resonant energy migration rate of $^2H_{11/2}$, taking into account the Boltzmann factor, is as large as 5.0×10^8 s^{-1}. This means that statistically the energy will migrate 130 times before the CR process $CR_{6\rightarrow3,0\rightarrow1}$ happens. As a result, the energy migration process may bring the energy to a quenching site which therefore increases the quenching rate.

In addition to the CR of the $^4S_{3/2}$ energy state, at high dopant ion concentrations, additional depopulation mechanisms are possible. In fact, emission from the $^2H_{9/2}$ (24 479 cm^{-1}) and $^2P_{3/2}$ (32 773 cm^{-1}) states has been observed. These states are populated by upconversion processes which also deplete the $^4S_{3/2}$ state [20].

4.2. The upconversion processes of $^4I_{13/2}$ and $^4I_{11/2}$ states

The energy separation between $^4I_{13/2}$ and $^4I_{15/2}$ is ∼6500 cm^{-1} and the transition between these two levels is dominated by the radiative process. Hence, the lifetime of $^4I_{13/2}$ is the

longest one in comparison with those of other Er^{3+} energy levels. The observed lifetime falls in the range 5.3–7.2 ms [18]. An efficient three-micrometre room-temperature laser emission from a much shorter lifetime of the emitting level $^4I_{11/2}$ to this level was obtained for $YAlO_3$ with a high concentration of Er^{3+} [19, 50]. The lifetime of the $^4I_{11/2}$ state is 0.9–1.2 ms and is a few times smaller than the $^4I_{13/2}$ lifetime. The lifetime decreases to 0.1 ms when the Er^{3+} dopant ion concentration is 45%. For YAG, the lifetime of the upper laser level, $^4I_{11/2}$, is 10 times shorter than the lower laser level $^4I_{13/2}$.

4.3. The upconversion process of $^4I_{13/2}$ states

Two models have been proposed to explain the absence of the self-saturation of the 3 μm lasing transition, namely excited state absorption (ESA) from the terminal laser level and cooperative upconversion:

$$UC_{1\to 0,1\to 3}: [^4I_{13/2}, {}^4I_{13/2}] \to [^4I_{15/2}, {}^4I_{9/2}] \qquad (-44, +1343\ \mathrm{cm}^{-1}). \quad (25)$$

Experimental evidence favours the latter [51, 52], in which the donor ion terminates in the ground electronic state and the acceptor ion is excited to $^4I_{9/2}$. Subsequent nonradiative relaxation of $^4I_{9/2}$ will then populate the initial 3 μm lasing state, $^4I_{11/2}$. For YAG (doped with 50 at.% Er^{3+}), the experimentally measured ET rates of this process (25) are between 2.5×10^{-17} and 1.3×10^{-15} $cm^3\ s^{-1}$ [53], and these values vary by two orders.

For $YAlO_3$:Er the experimentally measured ET rates for process (25), for 10, 15, and 25 at.% Er^{3+} doping were 7.5×10^{-18}, 2.5×10^{-17} and 5×10^{-17} $cm^3\ s^{-1}$, respectively [53]. Since for 1.5 at.% Er^{3+}, ρ equals 2.9×10^{20} cm^{-3} [9], the corresponding ET rates (s^{-1}) are given as $1.45 \times 10^4 \times P_a(^4I_{13/2})$, $7.25 \times 10^4 \times P_a(^4I_{13/2})$, and $2.42 \times 10^5 \times P_a(^4I_{13/2})$, respectively. Since the cutoff frequency of the phonon spectrum is $\approx$800 cm^{-1} [22], the upconversion process (25), $UC_{1\to 0,1\to 3}$ can be bridged by the emission of one phonon of energy 750 cm^{-1}.

It is difficult to calculate the exact magnitude of the upconversion rate of (25), $UC_{1\to 0,1\to 3}$, because it depends on the population $P_a(^4I_{13/2})$ of the acceptor Er^{3+} ion in the $^4I_{13/2}$ metastable state. As noted from table 1, all the interaction mechanisms, dd, dq, qd, and qq, contribute to the ET process. The calculated upconversion rate to one Er^{3+} ion in the first, second and third nearest shells are 3.5×10^5, 2.6×10^4 and 6.1×10^3 s^{-1}, respectively. Hence, for doping concentration $\geqslant$15%, i.e. when statistically there is at least one Er^{3+} acceptor ion in the distance of the first nearest neighbour, the ET rate to an acceptor ion in the first shell is of the magnitude $3.5 \times 10^5 \times P_a(^4I_{13/2})$. For low dopant ion concentration in the range of 5%–15%, the acceptor ion will be more likely located at the second nearest neighbour distance relative to the donor ion. Hence, the ET rate to this acceptor ion will be of the magnitude $2.6 \times 10^4 \times P_a(^4I_{13/2})$. This implies that for the dopant ion concentration increase from 10% to $\sim$20%, the ET rate will increase by 10 times. This is consistent with the experimental result that the ET rate for 10% Er^{3+} doping is one order smaller than the ET rate for 15% and 25% doping. The total ET rate is obtained by summing over all the numbers of nearest neighbours, and equals to $2.4 \times 10^6 \times C_{Er} P_a(^4I_{13/2})$.

4.4. The upconversion process of $^4I_{11/2}$ states

The next energy level state we investigate is the upper laser level of the 3 μm laser, $^4I_{11/2}$, for which the baricentre is only at 2231 cm^{-1} below that of the $^4I_{9/2}$ multiplet, so that nonradiative relaxation to $^4I_{11/2}$ is very efficient. In fact, these two energy multiplets have been approximated as a single one in some studies, for example [45].

In this section, we focus upon the calculation of the ratio of the upconversion rate of $^4I_{11/2}$ to that of $^4I_{13/2}$, $q = 1.87$, obtained experimentally by Georgescu *et al* [44]. These authors

attributed the upconversion process of $^4I_{11/2}$ to the following:

$$UC_{2\to0,2\to7}: [^4I_{11/2}, {}^4I_{11/2}] \to [^4I_{15/2}, {}^4F_{7/2}] \qquad (-637, +322\ \mathrm{cm}^{-1}). \quad (26)$$

Based upon our calculated matrix elements listed in table 1, we found that the qq and qd interactions are the dominant mechanisms. The ET rate to the first nearest neighbour Er^{3+} ion due to these two mechanisms is $\sim 5.2 \times 10^5\ \mathrm{s}^{-1}$. Using equation (15), we find that the upconversion rate of process $UC_{2\to0,2\to7}$ is $1.4 \times 10^6 \times C_{Er} P_a(^4I_{11/2})$, which is less efficient than process $UC_{1\to0,1\to3}$ by a factor of 1.8, so that q is 0.56. In view of this, we need to consider the possibility of the existence of another transfer pathway. We then note that there is another possible ET pathway that may contribute to the upconversion process, where the acceptor ion is upconverted to $^2H_{11/2}$ instead of to $^4F_{7/2}$. The baricentre of $^2H_{11/2}$ is 1370 cm^{-1} below that of $^4F_{7/2}$ and this ET process is:

$$UC_{2\to0,2\to6}: [^4I_{11/2}, {}^4I_{11/2}] \to [^4I_{15/2}, {}^2H_{11/2}] \qquad (+745, +1685\ \mathrm{cm}^{-1}). \quad (27)$$

When we take this ET process involving the emission of two phonons to compensate a mismatch of 1050 cm^{-1}, we find that $\alpha = 4.5 \times 10^{-3}$ and $\beta = 3.2 \times 10^{-3}$ (which are close to the values for process $CR_{5\to2,0\to1}$), so the ET rate of this process is $4.7 \times 10^6 \times C_{Er} P_a(^4I_{11/2})$, which is faster than process $UC_{2\to0,2\to7}$ by a factor of 3.4. Summing the ET rates of processes $UC_{2\to0,2\to7}$ and $UC_{2\to0,2\to6}$, and dividing the result by the ET rate of process $UC_{1\to0,1\to3}$, then we find $q = 2.5$ which is in good agreement with the result obtained in [44].

The reason that process $UC_{2\to0,2\to6}$ is efficient is because the squared reduced matrix element of $|\langle {}^2H_{11/2}||U^{(2)}||{}^4I_{11/2}\rangle|^2 = 0.0357$ is comparatively large, which is an order larger than $|\langle {}^4F_{7/2}||U^{(2)}||{}^4I_{11/2}\rangle|^2 = 0.0035$. Since both of the quadrupole transitions of the donor and acceptor ions for the process $UC_{2\to0,2\to6}$ are large, qq interaction is the dominant interaction mechanism and the corresponding ET rate to the nearest acceptor ion is found to be $2.0\times10^5\,\mathrm{s}^{-1}$.

5. The concentration dependence of the lifetime of the $^4I_{9/2}$ state

Finally, we consider the ET processes of the $^4I_{9/2}$ multiplet of Er^{3+} in $YAlO_3$, which plays a very important role in the 3 μm laser. Almost all of the excitation of the $^4I_{11/2}$ initial lasing multiplet is channelled through $^4I_{9/2}$. The lifetime of $^4I_{9/2}$ is observed to be 1 μs [18]. This short lifetime results from nonradiative decay to $^4I_{11/2}$ lying at 2231 cm^{-1} below $^4I_{9/2}$. The multiphonon relaxation rate at 300 K was estimated to be as large as $6 \times 10^5\ \mathrm{s}^{-1}$ [18].

Since the main decay channel of $^4I_{9/2}$ is through $^4I_{11/2}$, these two energy levels are commonly treated as a single level. However, this model is only true for the regime of low dopant ion concentration. At high concentrations of Er^{3+}, the concentration quenching of the $^4I_{9/2}$ level has been observed [54]. This has the detrimental effect that there is an increase of the oscillation threshold for a 50 at.% Er^{3+} laser rod, compared with a 30 at.% Er^{3+} one. A less dramatic threshold increase with concentration was obtained for pumping into $^4I_{11/2}$. In [54], the luminescence lifetime of $^4I_{9/2}$ was measured for different Er^{3+} dopant ion concentrations, with pumping into $^4I_{9/2}$. It was observed that the lifetime of $^4I_{9/2}$ decreased from 435 to 380 ns when the Er^{3+} concentration increased from 1 to 45 at.%. As a consequence, besides the feeding of the initial lasing multiplet $^4I_{11/2}$ from $^4I_{9/2}$ via multiphonon relaxation, the energy may cross-relax or upconvert to other states, resulting in the concentration quenching of $^4I_{9/2}$ for high Er^{3+} doping concentration. The processes involved are [54]:

$$CR_{3\to1,0\to1}: [^4I_{9/2}, {}^4I_{15/2}] \to [^4I_{13/2}, {}^4I_{13/2}] \qquad (-1343, +44\ \mathrm{cm}^{-1}), \quad (28)$$

and the upconversion processes:

$$U_{3\to0,3\to10}: [^4I_{9/2}, {}^4I_{9/2}] \to [^4I_{15/2}, {}^2G_{9/2}] \qquad (-496, +1025\ \mathrm{cm}^{-1}), \quad (29a)$$

Table 2. Experimentally determined merit factors of $^4I_{9/2}$ CR.

Er^{3+} at.%	1	3	5	15	20	45
τ_{exp} (ns)[a]	435	435	430	425	410	380
$CR_{3\rightarrow1,0\rightarrow1}$ (10^4 s^{-1})	0	0	2.6	5.3	14	33
h[a]	0	0	0.01	0.02	0.06	0.13

[a] From [54].

$$U_{3\rightarrow0,2\rightarrow9}: [^4I_{9/2}, {}^4I_{11/2}] \rightarrow [^4I_{15/2}, {}^4F_{3/2}] \qquad (-377, +618\ cm^{-1}), \qquad (29b)$$

$$U_{3\rightarrow9,2\rightarrow0}: [^4I_{9/2}, {}^4I_{11/2}] \rightarrow [^4F_{3/2}, {}^4I_{15/2}] \qquad (-618, +377\ cm^{-1}), \qquad (29c)$$

and energy migration to a quenching site.

For the process $CR_{3\rightarrow1,0\rightarrow1}$, both the donor and acceptor ions terminate in the $^4I_{13/2}$ terminal laser state, so that the threshold energy would be increased. This acts in opposition to the multiphonon relaxation process, $^4I_{9/2}$ to $^4I_{11/2}$, which enhances the lasing efficiency. In this CR process (28), a phonon of energy 750 cm^{-1} is required to bridge the energy mismatch and dq is the dominant interaction mechanism (see table 1). Using the HLO model, taking the doping concentration to be 45% and summing up to the first three shells of nearest neighbour ions, the ET rate equals 3.9×10^4 s^{-1}. A few relevant points should be noted here. This CR is a back transfer process of the upconversion of the $^4I_{13/2}$ state. Although the factor $P_a(^4I_{15/2})$ for the former case can be approximated by one under normal excitation, this ET process is endothermic and hence, the factor originating from the phonon part is smaller than that of the upconversion process of $^4I_{13/2}$ by two orders. Hence, in general, the back transfer process is slower than the $^4I_{13/2}$ upconversion process.

A low pump power was used in the study of [54] to turn off the upconversion process (29*a*). However, this may not be the case. Since the lifetime of the $^4I_{9/2}$ state is extremely short, then process (29*a*) has only a small rate, and the ET rate needs to be very fast in order to prevent the decay to $^4I_{11/2}$. As a result, it is more reasonable to say that at low pump power, the upconversion processes (29*b*) and (29*c*) are not important, where the Er^{3+} ion in $^4I_{9/2}$ interacts with a nearby ion in the excited state $^4I_{11/2}$ (that is achieved by decay from $^4I_{9/2}$). For process (29*b*), only the dd interaction is active and for process (29*c*), both the dd and dq interactions are active. With 45 at.% Er^{3+} doping, the ET rates of processes (29*b*) and (29*c*) are estimated to be $1.2 \times 10^4 \times P_a(^4I_{11/2})$ and $1.6 \times 10^5 \times P_a(^4I_{11/2})$ s^{-1}, respectively.

Finally, let us consider the contribution from the energy migration process. The interaction mechanisms involving a quadrupole transition in either the donor or acceptor ions are forbidden. Hence, the only contributing mechanism is dd interaction. Although it is a resonant process, the ET rate is estimated to be 9.3×10^3 s^{-1} for 45 at.% Er^{3+} concentration, which is not so important.

A merit factor, h, defined in [54] as the ratio of the CR rate from $^4I_{9/2}$, equation (28), to the total decay rate of $^4I_{9/2}$, is used to describe the detrimental effect of the CR $CR_{3\rightarrow1,0\rightarrow1}$ upon the lasing efficiency. For 45 at.% Er^{3+} doping concentration, h is 0.13 [54], and hence, 13% of the $^4I_{9/2}$ population will cross-relax to populate the $^4I_{13/2}$ level and increase the laser threshold. From these figures, the CR rate is estimated to be 3.3×10^5 s^{-1}. The experimentally determined CR rates for other dopant ion concentrations are tabulated in table 2. The ET rate roughly linearly depends on the doping concentration. Our calculated ET rate 3.9×10^4 s^{-1} due to the CR process, $CR_{3\rightarrow1,0\rightarrow1}$, is one order smaller than the measured one.

6. Conclusions

The upconversion of $^4I_{13/2}$ and $^4I_{11/2}$, and CR processes of $^4S_{3/2}$ for Er^{3+} in $YAlO_3$, which have important effects upon its 3 μm laser operation, have been investigated semi-quantitatively. The aim has been to identify dominant donor–acceptor ET channels, and other phenomena such as ESA [24, 55] and many body effects [56] have not been considered. The ET up to the third neighbouring shell has been considered. Generally, dq or qd and qq ET interaction mechanisms dominate over the dd mechanism. The qq interactions are particularly important in many of the ET pathways involving $^2H_{11/2}$, as well as the migration of energy in this state. Our theoretical treatment is complementary to the rate equation approach of Georgescu *et al* [54] who gave special attention to the detrimental effect of CR from $^4I_{9/2}$ upon the laser efficiency, but did not consider the role of $^2H_{11/2}$ in populating this level. We have found that the thermal population of the $^2H_{11/2}$ state is important in the quenching of '$^4S_{3/2}$' and the population of the $^4I_{9/2}$ term. For high doping concentration, energy migration in $^2H_{11/2}$ and subsequent transfer to trap sites, can lead to the quenching of $^4S_{3/2}$ emission. In addition to the upconversion process from $^4I_{11/2}$ to $^4F_{7/2}$ ($UC_{2\rightarrow 0,2\rightarrow 7}$) usually considered, the upconversion rate of $^4I_{11/2}$ to $^2H_{11/2}$ ($UC_{2\rightarrow 0,2\rightarrow 6}$) is 3.4 times greater, and hence both are needed for the explanation of the experimental results concerning the ratio of the upconversion rates of $^4I_{11/2}$ and $^4I_{13/2}$. Finally, the CR rate of $^4I_{9/2}$ has been estimated.

Acknowledgments

Financial support of this work is acknowledged under the Hong Kong Research Grants Council, Research Grant No CityU 1114/00P.

References

[1] Förster T 1948 *Ann. Phys., Lpz.* **2** 55
[2] Dexter D L 1953 *J. Chem. Phys.* **21** 836
[3] Kim G C, Mho S I and Park H L 1995 *J. Mater. Sci. Lett.* **14** 805
[4] Chivian J, Case W and Eden D 1979 *Appl. Phys. Lett.* **35** 124
[5] Kueny A, Case W and Koch M 1989 *J. Opt. Soc. Am.* B **6** 639
[6] Gumanskaya E G, Korzhik M V, Smirnova S A, Pavlenko V B and Fedorov A A 1991 *Opt. Spectrosc.* **72** 86
[7] Malinowski M, Garapon C, Joubert M F and Jacquier B 1995 *J. Phys.: Condens. Matter* **7** 199
[8] Zhang X, Jiang B, Yang Y and Wang Z 1997 *J. Appl. Phys.* **81** 6939
[9] Mares J A, Nikl M, Pedrini C, Moine B and Blazek K 1992 *Mater. Chem. Phys.* **32** 342
[10] Garcia M, Sibley W A, Hunt C A and Spaeth J M 1988 *J. Lumin.* **42** 35
[11] Mares A, Nikl M and Blazek K 1991 *Phys. Status Solidi* a **127** k65
[12] Mitsunaga M and Uesugi N 1991 *J. Lumin.* **48/49** 459
[13] Ni H and Rand S C 1991 *Opt. Lett.* **16** 1424
[14] Weber M J, Bass M, Andringa K, Monchamp R R and Comperchio E 1969 *Appl. Phys. Lett.* **15** 342
[15] Weber M J, Bass M and DeMars G A 1971 *J. Appl. Phys.* **12** 301
[16] Donlan V L and Santiago A A 1972 *J. Chem. Phys.* **57** 4717
[17] Weber M J 1973 *Phys. Rev.* B **8** 54
[18] Kaminskii A A, Mironov V S, Kornienko A, Bagaev S N, Boulon G, Brenier A and Di Bartolo B 1995 *Phys. Status Solidi* a **151** 231
[19] Stalder M, Lüthy W and Weber H P 1987 *Opt. Lett.* **12** 602
[20] Silversmith A J, Lenth W and MacFarlane R M 1987 *Appl. Phys. Lett.* **51** 1977
[21] Frauchiger J, Lüthy W, Albers P and Weber H P *Opt. Lett.* **13** 964
[22] Scheps R 1994 *IEEE J. Quantum Electron.* **30** 2914
[23] Scheps R 1995 *IEEE J. Quantum Electron.* **31** 309
[24] Pollnau M, Heumann E and Huber G 1994 *J. Lumin.* **60/61** 842
[25] Scheps R 1996 *Prog. Quantum Electron.* **20** 271

[26] Lupei V, Georgescu S and Florea V 1993 *IEEE J. Quantum Electron.* **29** 426
[27] Georgescu S, Lupei V, Glynn T J and Sherlock R 1994 *J. Lumin.* **60/61** 241
[28] Wang J and Simkin D J 1995 *Phys. Rev.* B **52** 3309
[29] Coppens P and Eibschutz M 1965 *Acta Crystallogr.* **19** 524
[30] Diehl R and Brandt G 1975 *MRS Bull.* **10** 85
[31] Wood R L and Hayes W 1982 *J. Phys. C: Solid State Phys.* **15** 7209
[32] Tomik T, Kaminao M, Tanahara Y, Futemma T, Fujisawa M and Fukudome F 1991 *J. Phys. Soc. Japan* **60** 1799
[33] Bertaut F and Mareschal J 1963 *C. R. Acad. Sci. Paris* **257** 867
[34] Vasylechko L, Akselrud L, Matkovskii A, Sugak D, Durygin A, Frukacz Z and Lukasiewicz T 1996 *J. Alloys Compounds* **242** 18
[35] Alain P and Piriou B 1971 *Phys. Status Solidi* b **43** 669
[36] Gupta H C and Ashdhir P 1999 *J. Solid State Chem.* **146** 287
[37] Kaminskii A A 1990 *Laser Crystals* (New York: Springer)
[38] Blaxha M G, Vylegzhanin D N, Kaminskii A A, Klokishner S I and Perlin Yu E 1976 *Izv. Akad. Nauk SSSR Ser. Fiz.* **40** 1851
[39] Kushida T 1973 *J. Phys. Soc. Japan* **34** 1318
[40] Holstein T, Lyo S K and Orbach R 1986 *Laser Spectroscopy of Solids* ed W M Yen and P M Selzer (New York: Springer) p 39
[41] Miyakawa T and Dexter D L 1970 *Phys. Rev.* B **1** 2961
[42] Yamada N, Shionoya S and Kushida T 1972 *J. Phys. Soc. Japan* **32** 1577
[43] Weber M J, Bass M, Varitimos T E and Bua D P 1973 *IEEE J. Quantum Electron.* **9** 1079
[44] Georgescu S, Lupei V, Trifan M, Sherlock R J and Glynn T J 1996 *J. Appl. Phys.* **80** 6610
[45] Brenier A and Jurdyc A M 1996 *J. Lumin.* **69** 131
[46] Perlin E, Kaminskii A A, Klokishner S I, Enakii V N, Bagdasarov K S, Bogomolova G A and Vylegzhanin D N 1977 *Phys. Status Solidi* a **40** 643
[47] Hoshina T 1967 *Japan. J. Appl. Phys.* **6** 1203
[48] Ofelt G S 1963 *J. Chem. Phys.* **38** 2171
[49] Faulkner T R and Richardson F S 1978 *Mol. Phys.* **35** 1141
[50] Wuthrich S, Lüthy W and Weber H P 1990 *J. Appl. Phys.* **68** 5467
[51] Kaminskii A A, Butaeva T I, Ivanov A O, Mochalov I V, Petrosyan A G, Rogov G I and Fedorov V A 1976 *Sov. Tech. Phys. Lett.* **2** 308
[52] Zhekov V I, Murina T M, Prokhorov A M, Studenikin M I, Georgescu S, Lupei V and Ursu I 1986 *Sov. Phys.—J. Quantum Electron.* **16** 274
[53] Breguet J, Umyskov A F, Semenkov S G, Lüthy W, Weber H P and Shcherbakov I A 1992 *IEEE J. Quantum Electron.* **28** 2563
[54] Georgescu S, Glynn T J, Sherlock R and Lupei V 1994 *Opt. Commun.* **106** 75
[55] Koetke J and Huber G 1995 *J. Appl. Phys.* B **61** 151
[56] Lupei A, Lupei V, Georgescu S, Ursu I, Zhekov V I, Murina T M and Prokhorov A M 1990 *Phys. Rev.* B **41** 10923